Research Square

Preprints are preliminary reports that have not undergone peer review.
They should not be considered conclusive, used to inform clinical practice,
or referenced by the media as validated information.

Biomimetic Setaria viridis-Inspired Co3O4/CoS Hierarchical Architecture on Carbon Cloth for Advanced Lithium Storage

Peng Lv
Jiamusi University
Zhiyang Gao
Jiamusi University
Tantan luo
Jiamusi University
Kuo Wang
Jiamusi University
Sheng Lin
Jiamusi University
Ming Hu
minghu02@jmsu.edu.cn
Jiamusi University
Meili Qi
Jiamusi University

Research Article

Keywords:

Posted Date: September 9th, 2026

DOI: https://doi.org/10.21203/rs.3.rs-10654910/v1

License: This work is licensed under a Creative Commons Attribution 4.0 International License.
Read Full License

Additional Declarations: No competing interests reported.

Version of Record: A version of this preprint was published at Research on Chemical Intermediates on November 14th, 2026. See the published version at https://doi.org/10.1007/s11164-026-06170-1.

Biomimetic Setaria viridis-Inspired Co_3O_4/CoS Hierarchical Architecture on Carbon Cloth for Advanced Lithium Storage

Peng Lv[1], Zhiyang Gao[1], Tantan luo[1], Kuo Wang[1], Sheng Lin[1], Ming Hu[1*], Meili Qi[1*]

[1] *School of Materials Science and Engineering, Jiamusi University, Jiamusi 154007, P. R. China*

E-mail address: lvpeng@jmsu.edu.cn(Peng Lv), jmsugaozhiyang@126.com(Zhiyang Gao), 17365491013@163.com(Tantan Luo), 18206897601@163.com (Kuo Wang), ls1451752109@outlook.com (Sheng Lin), minghu02@jmsu.edu.cn (Ming·Hu), meili8585@foxmail.com (Meili Qi),

ABSTRACT

To overcome the severe volume variation and intrinsically low electronic conductivity associated with Co_3O_4, a Co_3O_4/CoS@CC composite was constructed via sequential hydrothermal synthesis and electroprecipitation. This material employs flexible carbon cloth as the substrate, on which arrays of cobalt tetroxide (Co_3O_4) nanowires are first grown, followed by the electrodeposition of cobalt sulphide (CoS) onto the nanowire arrays. When evaluated lithium-ion batteries, the Co_3O_4/CoS@CC electrode delivered an initial discharge specific capacity of 1152.38 mA h g^{-1} at 0.1 A g^{-1}. After 200 charge-discharge cycles, it retained a reversible capacity of 613.07 mA h g^{-1} with a coulombic efficiency of 99.72%. Under a high loading current of 500 mA g^{-1}, the average discharge capacity reached 578.92 mA h g^{-1}. The biomimetic *Setaria viridis*-inspired hierarchical architecture endows the Co_3O_4/CoS@CC electrode with excellent long-term cycling durability and outstanding rate performance, which provides an enlarged specific surface area, an efficient conductive network, and improved structural robustness, thereby significantly enhancing the electrochemical performance.

1. Introduction

The widespread adoption of consumer electronics together has greatly increased the demand for lithium-ion batteries (LIBs), thereby stimulating extensive research on high-performance electrode materials[1-5]. Co_3O_4 is regarded as a promising

* Corresponding author. Tel.:+86 04548618703

E-mail address: minghu02@jmsu.edu.cn (Ming·Hu), meili8585@foxmail.com (Meili Qi),

representative of transition-metal oxides because it combines a high theoretical lithium-storage capacity with excellent redox activity, environmental benignity, and cost-effectiveness [6]. Nevertheless, the practical application of Co_3O_4 as a standalone anode material is hindered by its intrinsically low electrical conductivity, insufficient utilization of active species, and the substantial gap between the experimentally obtained capacity and its theoretical storage capability, particularly under large current loads or fast scan conditions [7, 8]. Integrating Co_3O_4 with other functional materials provides a practical route to overcoming these intrinsic limitations. In particular, transition metal sulfides (TMS), especially cobalt sulfide (CoS), have been extensively explored because they possess high theoretical capacity together with superior electrical conductivity [9-11]. Despite these advantages, substantial volume fluctuations during repeated cycling gradually disrupt the structural integrity of the electrode, thereby compromising cycling durability and rate performance [12-14]. The introduction of nanostructured CoS provides abundant interfacial exposure and abundant electrochemically accessible regions, thereby accelerating charge transfer and Li^+ migration while effectively relieving stress-induced structural deterioration [15, 16].

Carbon cloth (CC) is composed of an interconnected network of micron-sized carbon fibers, forming a stable conductive framework that provides continuous electron transport pathways for active materials while reducing interfacial resistance. In addition to its excellent electrical conductivity, CC exhibits remarkable flexibility and mechanical robustness, making it an attractive current collector for flexible energy storage devices [17, 18]. Its three-dimensional porous architecture provides abundant space for accommodating electroactive components, including cobalt sulfide and silicon-based materials, etc., while simultaneously facilitating electrolyte infiltration and lithium-ion transport. Furthermore, the interconnected porous framework provides sufficient space to buffer the repeated expansion and contraction of the electrode during electrochemical cycling. These structural and electrochemical merits make carbon cloth an attractive platform for the construction of next-generation electrode architectures [19, 20].

In this study, three-dimensional (3D) Co_3O_4/CoS array electrodes were fabricated on CC through integrating hydrothermal growth with a subsequent electrodeposition

process to develop high-performance lithium-storage electrodes. Initially, Co_3O_4 was directly formed as aligned nanowire arrays across the surface of the CC support through a single hydrothermal treatment. Subsequently, CoS nanoparticles were deposited onto the Co_3O_4 nanowire arrays by electrodeposition, yielding the Co_3O_4/CoS composite array architecture. Benefiting from this integrated structure, the as-prepared Co_3O_4/CoS composites supported on CC exhibited outstanding electrochemical performance.

2. Experiments

2.1 Materials

Commercially available hydrophilic CC was employed as the supporting substrate for the electrode. The synthesis was carried out using cobalt nitrate hexahydrate ($Co(NO_3)_2 \cdot 6H_2O$), urea ($CO(NH_2)_2$), ammonium fluoride (NH_4F), cobalt chloride hexahydrate ($CoCl_2 \cdot 6H_2O$), and thiourea (H_2NSNH_2), all of which were purchased from Suzhou Willett Environmental Technology Co. No purification or pretreatment was applied to any of the chemicals before use.

2.2 Preparation of Co_3O_4/CC nanowire arrays

A hydrothermal process was employed to obtain the Co_3O_4/CC composite. To formulate the reaction precursor, 2 mmol of $Co(NO_3)_2 \cdot 6H_2O$, 12 mmol of NH_4F, and 20 mmol of $CO(NH_2)_2$ were dissolved in 40 mL of DI and maintained under continuous stirring at ambient temperature for 30 min. A piece of carbon cloth immersed in the resulting precursor solution was loaded into a 50 mL Teflon-lined hydrothermal reactor. Crystal growth was induced by heating the sealed reactor at 110 °C for 5 h. Upon completion of the hydrothermal treatment, the reactor was left to return to ambient temperature naturally prior to opening. The carbon cloth carrying the as-prepared precursor was then removed, thoroughly cleaned with deionized water until no residual reactants, and placed in an oven at 60 °C for 3 h. Finally, thermal conversion of the precursor into Co_3O_4 was accomplished by heating the precursor-coated carbon cloth to 350 °C under a continuous N_2 at a ramping rate of 5 °C min^{-1}, followed by a 2 h dwell at the target temperature to obtain the Co_3O_4/CC composite.

2.3 Preparation of Co_3O_4/CoS@CC nanowire arrays

The Co_3O_4/CoS@CC sample was fabricated by electrodeposition using a conventional three-electrode configuration. An electrolyte containing $CoCl_2 \cdot 6H_2O$

(0.05 M) and H_2NSNH_2 (1.0 M) was first prepared for the deposition process. The Co_3O_4/CC sample was connected as the working electrode, while a platinum plate and Ag/AgCl electrode were used to complete the electrochemical cell. CoS growth was achieved by CV deposition over a potential window ranging from -1.2 V and 0.2 V with 10 mV S^{-1}, and the deposition procedure was repeated for eight consecutive cycles. Upon completion of electrodeposition, the coated CC was sequentially washed using ethanol followed by DI to remove residual electrolyte, after which it was placed in a vacuum oven maintained at 60 °C for 3 h.

2.4 Instrumentation

Structural information was obtained from X-ray diffraction measurements performed on a Rigaku Dmax-2000 diffractometer employing CuKα radiation. The microscopy of the synthesized materials and the spatial distribution of the constituent elements were examined using a JEOL JMS-7800F field-emission scanning electron microscope equipped with an energy-dispersive X-ray spectroscopy detector. X-ray photoelectron spectroscopy (ESCALAB250) was employed to probe the chemical environment and electronic states of the surface elements.

2.5 Electrochemical evaluation

The electrochemical properties of the prepared electrodes were evaluated in CR2032 coin cells. All assembly procedures were completed inside an argon atmosphere under ultra-low oxygen and moisture conditions (O_2 and $H_2O < 0.01$ ppm). The cell configuration consisted of the prepared electrode, lithium metal foil, and a Celgard 2400 separator. Galvanostatic charge/discharge (GCD) experiments were carried out using a NEWARE multichannel battery analyzer between 0.01 and 3.0 V (vs. Li/Li^+), and CV was acquired on a CHI660e instrument at 0.1 mV s^{-1} over the same voltage window. The impedance response of the cells was subsequently analyzed by electrochemical impedance spectroscopy within the frequency range from 10^{-2} to 10^6 Hz.

3. Results and discussion

The Co_3O_4/CoS@CC composite was constructed through sequential hydrothermal growth and electrodeposition, as illustrated in Figure 1. Initially, ammonium fluoride was introduced as a structure-directing agent to enable the in situ hydrothermal growth of the Co_3O_4 precursor on the CC substrate. After subsequent heat treatment, well-

defined Co_3O_4 nanowire arrays were obtained. The Co_3O_4/CoS@CC composite was then fabricated by depositing CoS on the Co_3O_4 nanowire arrays through an electrodeposition process. For convenience, the Co_3O_4/CC and Co_3O_4/CoS@CC electrodes are referred to as Sample A and Sample B, in the following figure captions.

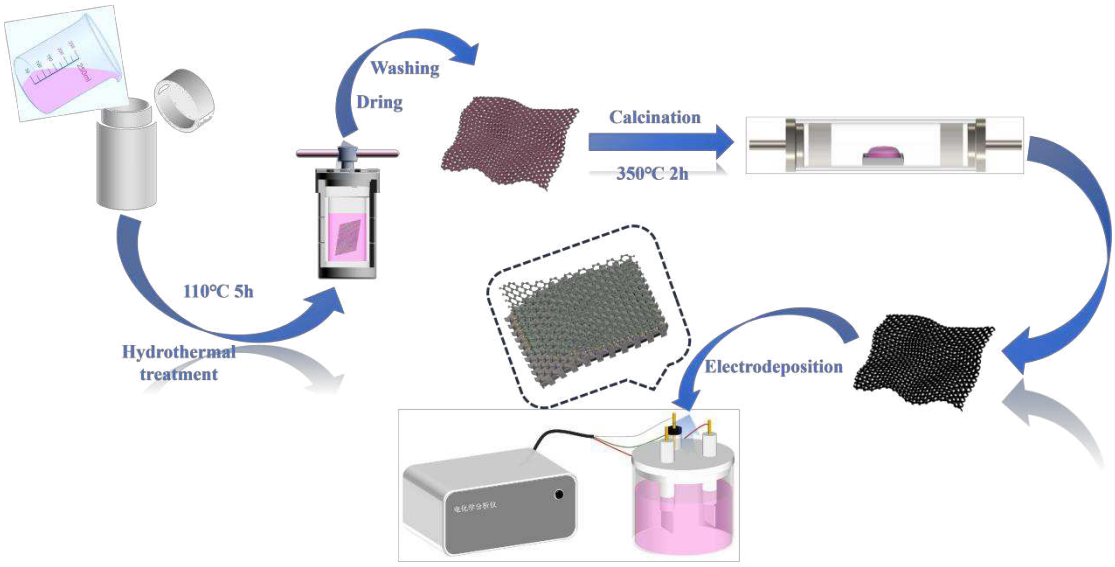


Figure 1 Sequential preparation procedure for constructing Sample A and Sample B.

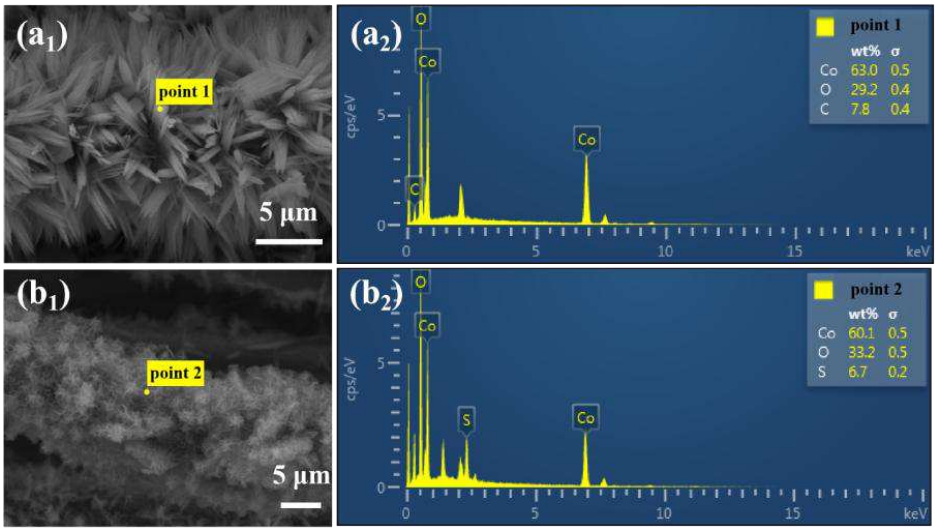


Figure 2. FE-SEM images and point EDS spectra of the two samples: (a_1, a_2) Sample A; (b_1, b_2) Sample B.

The morphological characteristics and elemental composition of Samples A and B were investigated by FE-SEM coupled with point EDS analysis, as illustrated in Figure 2. As shown in Figures 2a_1 and 2a_2, the Co_3O_4/CC electrode is composed of densely distributed nanowire arrays with uniform dimensions and homogeneous morphology.

Statistical measurements indicate that the nanowires are approximately 3.3 μm in length, while the average tip diameter is about 0.5 μm. The corresponding point EDS spectrum confirms Co, O, and C as the major elemental constituents of Sample A. Following electrodeposition, the morphology of the nanowire arrays is retained, while the point EDS spectrum of Sample B, shown in Figures $2b_1$ and $2b_2$, reveals the coexistence of Co, O, and S, indicating the successful introduction of the sulfide phase.

Representative FE-SEM images together with EDS elemental mapping of the Co_3O_4/CoS@CC composite after electrodeposition are displayedin Figure 3. As presented in Figures 3a and 3b, the surfaces of the Co_3O_4 nanowire arrays are densely covered with nanoscale flower-like structures, resulting in a distinctive biomimetic *Setaria viridis*-inspired hierarchical architecture. This hierarchical morphology is constructed from numerous interconnected nanosheets with a typical size of around 20 nm. Such a structure design effectively enlarges the specific surface area, thereby providing abundant electrochemical reaction interfaces while reducing the migration distance for both lithium ions and electrons. Moreover, the integration of two-dimensional nanosheets with one-dimensional nanowire arrays enhances the mechanical robustness of the electrode, mitigates active-material pulverization under repeated cycling, and consequently improves cycling stability [21, 22].

The corresponding EDS elemental mapping images (Figures 3e-h) demonstrate that the presence of Co, O, C, and S throughout the composite. All four elements are uniformly distributed throughout the electrode, while the S element is mainly concentrated on the surface of the nanowire arrays, providing direct evidence that CoS has been successfully deposited onto the Co_3O_4 nanowire arrays. To examine the morphological integrity of the composite during long-term electrochemical operation, the cell was disassembled after 200 cycles, and the resulting microstructural evolution is presented in Figure S1.

The morphology of the Co_3O_4/CoS@CC sample following 200 galvanostatic cycles at 0.1 A g^{-1} in Figure S1, that the original morphology undergoes noticeable degradation during prolonged cycling. Nevertheless, portions of the porous architecture remain intact, allowing the electrode to preserve a certain level of capacity after 200 cycles. The biomimetic *Setaria viridis*-inspired hierarchical structure effectively

buffers the mechanical strain associated with Li^+ insertion, thereby contributing to the structural stability of the electrode. However, the observed aggregation and collapse of the nanosheets suggest that repeated lithiation/delithiation gradually obscures the boundaries between adjacent nanosheets, leading to a reduction in the available reaction interface and fewer electrochemically accessible sites remain. This structural evolution represents responsible for the progressive loss in reversible capacity during cycling.

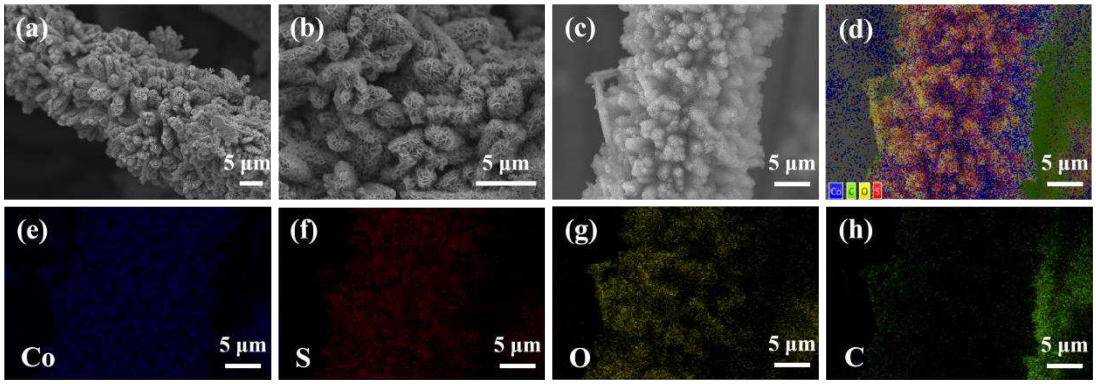


Figure 3 FE-SEM characterization of the Co_3O_4/CoS@CC composite: (a, b) SEM micrographs; (c-h) Corresponding elemental maps of Co, O, S, and C.

Figure 4a compares the XRD profiles of Samples A and B. For the Co_3O_4/CC sample, reflections located at 2θ = 31.3°, 36.8°, 44.8°, 59.4°, and 65.2°are assigned to the (220), (311), (400), (511), and (440) lattice planes of Co_3O_4 (PDF#43-1003), respectively [23]. Following the electrodeposition of CoS onto the Co_3O_4/CC electrode, these diffraction peaks exhibit a systematic shift. This behavior is mainly associated with the incorporation of cobalt sulfide, which promotes interfacial ion interdiffusion and/or solid-solution formation at the Co_3O_4/CoS interface. In particular, sulfide ions (S^{2-}) may interact with the Co_3O_4 lattice in the interfacial region, while changes in the valence state or coordination environment of cobalt ions can generate tensile stress within the lattice. Since S^{2-} possesses a larger ionic radius than O^{2-}, lattice expansion occurs, leading to an increase in the lattice constant [24]. Collectively, these structural features confirm the presence of the Co_3O_4/CoS heterostructure with a well-developed heterointerface.

XPS characterization was carried out to determine the elemental species and chemical environments in the Co_3O_4/CoS@CC composite. The survey spectrum (Fig.

4b) reveals the coexistence of Co, S, O, and C, indicating that all expected elements are incorporated into the fabricated material. Particular attention was first directed to the cobalt and sulfur regions because they provide direct evidence for the formation of the Co_3O_4/CoS heterostructure. As displayed in Fig. 4e, the Co 2p spectrum contains two spin-orbit doublets located at 779.79/781.18 eV and 795.65/797.04 eV, together with satellite features centered at 785.26 and 802.06 eV. The spin–orbit splitting energy is approximately 15.9 eV, which is characteristic of the coexistence of Co^{2+} and Co^{3+} oxidation states [25,26]. Correspondingly, the S 2p spectrum (Fig. 4f) can be resolved into three pairs of peaks. The doublet at 163.29 and 164.92 eV is assigned to C-S bonding, while the remaining doublets at 166.54/167.44 eV and 168.50/169.85 eV originate from SO_3^{2-} and SO_4^{2-} species, respectively [27,28]. These spectral features collectively verify the successful incorporation of the sulfide phase into the composite. In addition, three O 1s components (Fig. 4d) are resolved at 530.36, 531.29, and 532.69 eV, representing O_L, O_V, and O_{ads}, respectively. The C 1s spectrum (Fig. 4c) exhibits three characteristic contributions at 284.80, 286.05, and 289.19 eV, which are attributed to C-C, C-O, and C=O bonds, respectively [29]. Taken together, the XPS results provide convincing evidence for the coexistence of cobalt oxide and cobalt sulfide in the Co_3O_4/CoS@CC composite.

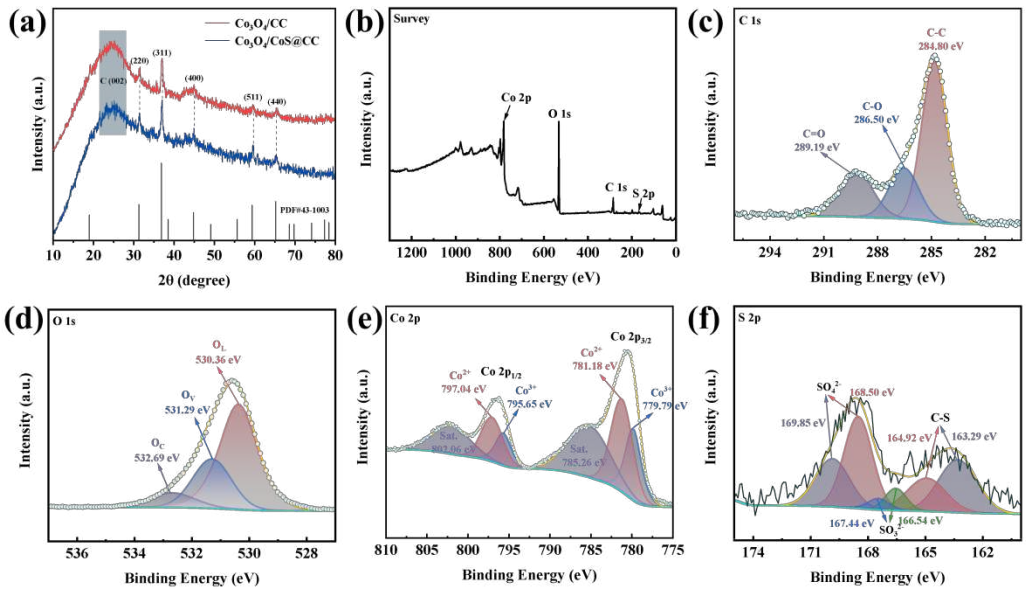


Figure 4 Structure and XPS analysis of the prepared samples.
(a)XRD results for Samples A and B; (b) Full-scan XPS spectrum of Sample B; (c-f) Deconvoluted core-level spectra corresponding to C 1s, O 1s, Co 2p, and S 2p.

The electrochemical behavior of the Co_3O_4/CoS@CC electrode was investigated using CV, where the potential was swept between 0.01 and 3.00 V at 0.1 mV s^{-1} (Figure 5a). The excellent overlap between the subsequent CV profiles indicates that stable and reversible redox behavior is established once the first-cycle activation is completed. In contrast, the first cycle exhibits obvious differences from the subsequent scans. Two cathodic peaks located at 0.82 and 0.43 V are observed during the initial lithiation process. The former is associated with the conversion of CoS into metallic Co accompanied by Li_2S formation, whereas the latter mainly originates from electrolyte decomposition together with the establishment of the SEI [1,30]. After the first cycle, the anodic peak is detected at 1.12 V, while the cathodic peaks appear at 0.58 and 1.72 V. The displacement of these characteristic peaks reflects the gradual activation of the electrode and the improved kinetics of the electrochemical reactions. The reduction (Equation (1)) and oxidation (Equation (2)) processes observed during cycling follow the electrochemical equations below. Accordingly, the reversible lithium-storage mechanism of Sample B is summarized in the corresponding reaction equations (Equation (3)) [13, 31].

$$CoS + 2Li^+ + 2e^- \rightarrow Co + Li_2S \quad (1)$$

$$Co + Li_2S \rightarrow CoS + 2Li^+ + 2e^- \quad (2)$$

$$CoS + 2Li^+ + 2e^- \rightarrow Co + Li_2S \quad (3)$$

Figures 5b and 5c present the constant-current cycling curves of Samples A and B measured at 100 mA g^{-1}. Compared with the Co_3O_4/CC electrode, the Co_3O_4/CoS@CC electrode exhibits substantially enhanced lithium-storage capability throughout the cycling process. In the initial cycle, the discharge/charge capacities reach 1152.36/1146.67 mA h g^{-1}, whereas the corresponding values for Co_3O_4/CC are only 930.89/926.53 mA h g^{-1}. Part of the lithium inventory is irreversibly consumed during the first cycle because of SEI generation and concurrent parasitic reactions, leading to the discrepancy during the initial lithiation process [32, 33]. With continued cycling, the constant-current cycling curves of the Co_3O_4/CoS@CC electrode become highly reproducible and nearly coincide, demonstrating its excellent electrochemical reversibility as a LIB anode. After 200 cycles, the Co_3O_4/CoS@CC electrode retained reversible capacities as high as 613.09/611.38 mA h g^{-1} (discharge/charge), whereas the

Co_3O_4/CC electrode delivered only 213.20/211.71mA h g^{-1}. Such electrochemical behaviors reflect the excellent redox reversibility and long-term cycling durability of the Co_3O_4/CoS@CC composite electrode.

The cycling performance of Samples A and B measured at 100 mA g^{-1} is illustrated in Figure 5d. The Co_3O_4/CoS@CC electrode delivered 1152.38 mA h g^{-1} in its first discharge process. During prolonged cycling, the capacity initially decreased, subsequently increased, and finally exhibited a gradual decline. Despite this evolution, a high discharge capacity of 613.07 mA h g^{-1} was retained 200 cycles, accompanied by a coulombic efficiency of 99.72 %. In contrast, the Co_3O_4/CC electrode exhibited 930.90 mA h g^{-1} in the first discharge process, with the capacity showing an initial increase followed by continuous decay, ultimately retaining only 213.20 mA h g^{-1} by the 200th cycle while maintaining the coulombic efficiency of 99.77 %. The characteristic cycling behavior of the Co_3O_4/CoS@CC electrode reflects a typical "negative activation" or "activation-failure" process. At the early stage of cycling, interfacial side reactions consume part of the active lithium and generate a SEI, giving rise to the initial capacity decrease. This process consumes both electrolyte and lithium ions, leading to irreversible capacity loss during the early cycles [34]. In addition, residual impurities or metastable phases remaining on the electrode surface may participate in irreversible side reactions, further contributing to the initial decline. For the Co_3O_4/CoS@CC electrode, the gradual recovery in capacity is mainly ascribed to the progressive wetting of its hierarchical porous architecture by the electrolyte, allowing both Co_3O_4 and CoS to become increasingly involved in the electrochemical reactions [35]. Furthermore, CoS may experience lattice reconstruction or phase transformation during the initial cycling process, exposing additional electrochemically active sites and thereby gradually enhancing the reversible capacity [36]. The final capacity fading observed after extended cycling is primarily attributed to structural degradation, including weakened interfacial adhesion, pulverization or partial detachment of the CoS layer, and a substantial increase in contact resistance between the carbon cloth substrate and the active material, all of which accelerate the deterioration of electrochemical performance [7]. Notably, the onset of the capacity recovery stage for the Co_3O_4/CoS@CC electrode occurs later than that of the Co_3O_4/CC

electrode. This delayed activation behavior is also consistent with the existence of the deposited CoS layer on the Co_3O_4 framework.

Figure 5e compares the rate capabilities of Samples A and B under stepwise current loading. For the Co_3O_4/CC electrode, the average discharge specific capacities reached 1105.88, 873.68, 738.88, and 578.92 mA h g^{-1} when the applied current was sequentially increased from 0.1, 0.2, 0.3, and 0.5 A g^{-1}. Under the same testing conditions, the Co_3O_4/CC electrode delivered lower average discharge specific capacities of 874.88, 662.81, 563.75, and 456 mA h g^{-1}. When the applied current was restored to 0.1 A g^{-1}, the Co_3O_4/CoS@CC electrode still recovered 871.38 mA h g^{-1}, demonstrating its excellent reversibility under varying current densities. The enhanced rate response is closely related to the hierarchical Co_3O_4/CoS architecture. The CoS nanosheets expose additional reaction interfaces and establish more efficient electron/ion transport pathways, while the porous heterostructure facilitates electrolyte penetration and alleviates polarization during high-rate cycling, thereby maintaining rapid reaction kinetics even under increased current loads [37].

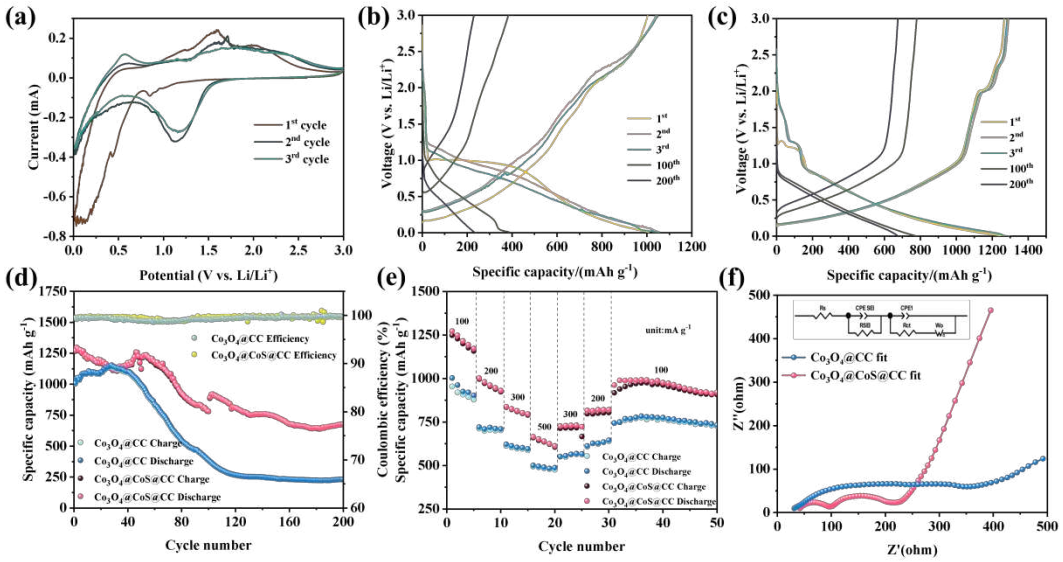


Figure 5 Electrochemical performance of Samples A and B: (a) Cyclic voltammograms of Sample B; (b, c) GCD profiles at 100 mA g^{-1}; (d) Cycling stability at 100 mA g^{-1}; (e) Rate capability under different current loads; (f) Nyquist spectra acquired after 100 cycles.

To clarify the kinetic differences between the two electrodes, EIS measurements were performed, and the corresponding Nyquist plots are displayed in Figure 5f. The impedance profiles were analyzed using the equivalent electrical circuit shown in the inset, from which the ohmic resistance (Rs), interfacial film resistance (R_{SEI}), and

charge-transfer resistance (R_{CT}) were determined. Compared with the Co_3O_4/CC electrode, the Co_3O_4/CoS@CC electrode exhibits a markedly lower R_{SEI} (56.68 Ω versus 259.8 Ω) and a dramatically reduced R_{CT} (104 Ω versus 2250 Ω), indicating substantially accelerated interfacial charge transport after CoS deposition. The reduced interfacial resistance can be ascribed to the conductive CoS shell and the intimate Co3O4/CoS heterointerface, which together facilitate electron transport, accelerate Li^+ migration across the electrode/electrolyte interface, and suppress electrochemical polarization during cycling [38]. These results demonstrate that the incorporation of CoS effectively improves the charge transport pathways within Sample B. Moreover, the low-frequency region of Sample B exhibits a steeper and more nearly vertical line than that of Sample A, suggesting faster lithium-ion diffusion in the electrolyte and enhanced diffusion kinetics within the composite electrode [39]. Taken together, the impedance analysis confirms that introducing CoS effectively optimizes the electrochemical reaction environment of the electrode.

Figure 6a presents a series of photographs recorded during the dynamic contact-angle measurement. Immediately after the electrolyte droplet contacted the electrode surface, continuous spreading was observed. By 19.4 s, the droplet had completely infiltrated the electrode, and the final contact angle was below 90°, indicating complete wetting of the electrode surface. These observations demonstrate the excellent hydrophilicity of the Co_3O_4/CoS@CC composite. The superior wettability can originate from the combination of the interconnected porous carbon cloth framework and the in situ constructed hierarchical Co_3O_4/CoS heterostructure which together form continuous pore channels that markedly enhance electrolyte infiltration and retention. Improved wettability enables Li^+ to access the active material more readily, strengthens electrolyte–electrode interfacial contact, minimizes resistance associated with interfacial charge transfer, and thereby accelerates the overall electrochemical process. Consequently, the above structural and interfacial features provide a reasonable explanation for the remarkable electrochemical performance of Sample B under both prolonged cycling and high-current operation.

Figure 6b presents a photograph of Sample B under a bending condition. Even when the electrode was bent to a large angle using tweezers, neither detachment of the

active material nor fracture of the carbon cloth substrate was observed, demonstrating that the composite effectively inherits the outstanding mechanical flexibility of the carbon cloth support. This excellent mechanical durability is attributed to the interconnected carbon fiber network, which provides high structural integrity and exceptional tolerance to mechanical deformation. Meanwhile, the Co_3O_4/CoS nanoarchitecture formed directly on the carbon cloth remains mechanically integrated with the substrate, minimizing the detachment of electrochemically active species arising from repeated expansion and contraction. Ultimately, the Co_3O_4/CoS@CC composite exhibits the mechanical robustness required for application in flexible energy storage devices.

As illustrated in Figure 6c, a CR2032 coin cell assembled with the Co_3O_4/CoS@CC electrode is capable of continuously powering multiple LED indicators for up to 2 h, demonstrating its reliable electrochemical output and excellent energy-storage capability under practical operating conditions. Combined with the superior wettability and outstanding mechanical flexibility discussed above, this device further confirms direct evidence for the promising electrochemical behavior of Sample B. These results collectively highlight the considerable potential of Sample B for practical and industrial applications in lithium-ion energy storage systems.

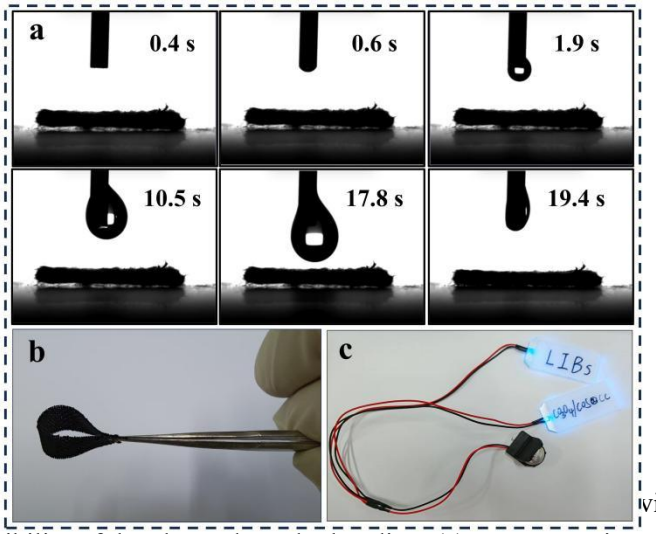


Figure 6 Physical c vior. (b) Photograph showing the flexibility of the electrode under bending. (c) Demonstration of the assembled CR2032 coin cell powering multiple LEDs.

4. Conclusions

In this work, a Co_3O_4/CoS@CC composite was successfully fabricated through a

straightforward combination of hydrothermal synthesis and electrodeposition. The introduction of the CoS nanoflower architecture effectively increases the specific surface area, improves electrical conductivity, promotes Li^+ transport, and buffers the volume variation associated with repeated charge-discharge processes. Owing to these structural advantages, the Co_3O_4/CoS@CC composite exhibits outstanding lithium-storage behavior. Even after 200 cycles at 0.1 A g^{-1}, the electrode maintained a capacity of 613.07 mA h g^{-1}, far exceeding the value of 213.20 mA h g^{-1} obtained for the Co_3O_4/CC electrode. The favorable lithium-storage performance primarily arises from the abundant redox-active sites and superior electronic conductivity provided by CoS. In the composite architecture, Co_3O_4/CC serves as the supporting framework, while electrodeposited CoS as nanosheets are uniformly distributed over the Co_3O_4 nanowire arrays. This hierarchical configuration facilitates electrolyte infiltration and charge transport, while simultaneously buffering the dimensional variation generated during repeated cycling. Furthermore, the present study offers a facile strategy for the preparation of ultrafine CoS nanosheets. Benefiting from its flexibility, sustained electrochemical output, and long-term operational durability, the resulting Co_3O_4/CoS@CC composite demonstrates considerable potential for practical lithium-ion battery applications.

Authors Contributions: P.L. contributed to experimental design, data curation, writing—original draft. K.W. contributed to conceptualization. T.L. and Z.G. contributed to data analyses. S.L. contributed to investigation. M.Q. funding acquisition methodology, investigation, formal analysis. M.H. contributed to experimental design, resources, investigation, and validation. All authors have read and agreed to the published version of the manuscript.

Funding: The authors acknowledge financial Supported by Heilongjiang Provincial Natural Science Foundation of China (PL2025E022); Supported By Program for Young Talents of Basic Research in Universities of Heilongjiang Province (YQJH2023227); Basic Scientific Research Expenses Project of Universities in Heilongjiang (2023-KYYWF-0571).

Institutional Review Board Statement: Not applicable

Informed Consent Statement: Not applicable

Data Availability Statement: The data that support the findings of this study are available on request from the corresponding author.

Conflicts of Interest: The authors declare that they have no known competing financial interests or personal relationships that could have appeared to influence the work reported in this paper.

References

[1] Zhang X, Wang K, Qiu J, Tian M, Yip J, Hao Z, Xu G (2024) Pristine cobalt humic acid xerogels embedded with ultrafine cobalt sulfide for enhanced and stable lithium-ion storage. J Colloid Interf Sci 663: 902-908. https://doi.org/10.1016/j.jcis.2024.02.207

[2] Chang H, WU Y, Han X, Yi T (2021) Recent developments in advanced anode materials for lithium-ion batteries. Energy Mater-us 1: 100003. https://doi.org/10.20517/energymater.2021.02

[3] Xie L, Tang C, Bi Z, Song M, Fan Y, Yan C, Li X, Su F, Zhang Q, Chen C (2021) Hard carbon anodes for next-generation Li-ion batteries: review and perspective. Adv Energy Mater 11: 2101650. https://doi.org/10.1002/aenm.202101650

[4] Tian M, Hao Z (2023) Synthesis of vanadium-doped Ti_3C_2Tx MXene for enhanced lithium storage. Funct Mater let 16: 2340006.https://doi.org/10.1142/S1793604723400064

[5] Chen W, Kuang S, Wei H, Wu P, Tang T, Li H, Liang Y, Yu X, Yu J (2022) Dual carbon and void space confined SiO_x/C@void@Si/C yolk-shell nanospheres with high-rate performances and outstanding cyclability for lithium-ion batteries anodes. J Colloid Interf Sci 610: 583-591. https://doi.org/10.1016/j.jcis.2021.11.099

[6] Xia H, Tu J, Mai Y, Wang X, Gu C, Zhao X (2011) Self-supported hydrothermal synthesized hollow Co_3O_4 nanowire arrays with high supercapacitor capacitance. J Mater Chem 21: 9319-9325. https://doi.org/10.1039/C1JM10946D

[7] Ning J, Zhang T, He Y, Jia C, Saha P, Cheng Q (2017) Co_3O_4@CoS core-shell nanosheets on carbon cloth for high performance supercapacitor electrodes. Materials 10: 608. https://doi.org/10.3390/ma10060608

[8] Xia X, Tu J, Zhang Y, Mai Y, Wang X, Gu C, Zhao X (2012) Freestanding Co_3O_4 nanowire array for high performance supercapacitors. Rsc Adv 2: 1835-1841. https://doi.org/10.1039/C1RA00771H

[9] Xia T, Umar A, Wu X (2022) Transition metal sulfide/hydroxide electrode materials with high specific capacities. Materials Advances 3: 6246-6252. https://doi.org/10.1039/D2MA00653G

[10] Lu S, Wang Z, Zhang X, He Z, Tong H, Li Y, Zheng J (2020) In situ-formed hollow cobalt sulfide wrapped by reduced graphene oxide as an anode for high-performance lithium-ion batteries. ACS Appl. Mater. Interfaces 12: 2671-2678. https://doi.org/10.1021/acsami.9b18931

[11] Chen H, Li Y, Liu R, Zhang B, Han Z, Lau W, Lu Y, Wang X, Wang M, Zhou D (2023) Novel porous $CoS_{1.097}$@carbon nanofibers as flexible and binder-free anode material for sodium-ion

batteries. J Alloy Compd 956: 170341.https://doi.org/10.1016/j.jallcom.2023.170341

[12] Pang M, Song Z, Jiang S, Zhang R, Wu Z, Jiao Y, Zhou W, Zhao J (2025) N-doped ultrafine CoP/CoS nanoparticles anchored on the rGO lamellas as anode for enhanced lithium storage. Appl Surf Sci 709: 163805. https://doi.org/10.1016/j.apsusc.2025.163805

[13] Kong L, Liu Y, Huang H, Liu M, Xu W, Li B, Bu X (2021) Interconnected CoS_2/NC-CNTs network as high-performance anode materials for lithium-ion batteries. Science China Materials 64: 820-829. https://doi.org/10.1007/s40843-020-1477-0

[14] Wang J, Zhao Y, He C, Li K, Wang Z, Liu J, Zhang Q, Mao N, Cao Y (2024) Metal sulfides encapsulated in doped carbon aerogel towards superior and safe energy storage: two birds with one stone. Electrochim Acta 477: 143819. https://doi.org/10.1016/j.electacta.2024.143819

[15] Wang S, Qu C, Wen J, Wang C, Ma X, Yang Y, Huang G, Sun H, Xu S (2023) Progress of transition metal sulfides used as lithium-ion battery anodes. Mater Chem Front 7: 2779-2808. https://doi.org/10.1039/D2QM01200F

[16] Pan Y, Cheng X, Gong L, Shi L, Zhang H (2018) Nanoflower-like N-doped C/CoS_2 as high-performance anode materials for Na-ion batteries. Nanoscale 10: 20813-20820. https://doi.org/10.1039/C8NR06959J

[17] Wang Y, Wang Z, Xu Y, Chen W, Shao G, Hou B (2024) Targeted design strategies for a highly activated carbon cloth cathode/anode to construct flexible and cuttable sodium Ion capacitors with an all-woven-structure. Energ Environ Sci 17: 6811-6820. https://doi.org/10.1039/D4EE02578D

[18] Zhao N, Fu P, Cui X, Luo M, Huang J (2025) Electrodeposition of nickel cobalt layered double hydroxides on conductive nickel-coated carbon cloth: a strategy for boosting flexible supercapacitor electrode performance. J Energy Storage 110: 115355. https://doi.org/10.1016/j.est.2025.115355

[19] Zhang L, Huang T, Gong H (2017) Remarkable improvement in supercapacitor performance by sulfur introduction during a one-step synthesis of nickel hydroxide. Phys Chem Chem Phys 19: 10462-10469. https://doi.org/10.1039/C7CP01234A

[20] Zhang S, Xiao S, Li D, Liao J, Ji F, Liu H, Ci L (2022) Commercial carbon cloth: an emerging substrate for practical lithium metal batteries, Energy Storage Mater 48 172–190. https://doi.org/10.1016/j.ensm.2022.03.014

[21] Liu W, Zhao Y, Zheng J, Jin D, Wang Y, Lian J, Yang S, Li G, Bu Y, Qiao F (2022)

Heterogeneous cobalt polysulfide leaf-like array/carbon nanofiber composites derived from zeolite imidazole framework for advanced asymmetric supercapacitors. J colloid interf sci 606: 728-735. https://doi.org/10.1016/j.jcis.2021.08.066

[22] Xiao X, Zou L, Pang H, Xu Q (2020) Synthesis of micro/nanoscaled metal–organic frameworks and their direct electrochemical applications. Chem Soc Rev 49: 301-331. https://doi.org/10.1039/C7CS00614D

[23] Lv P, Li X, Li H, Liu Z, Hu M, Qi M (2025) Smart construction of Co_3O_4 nanowire arrays on carbon cloth of flexible electrodes toward enhanced Lithium-ion battery. ChemistrySelect 10: e02399. https://doi.org/10.1002/slct.202502399

[24] Zhang C, Xie J, Zhao C, Yang Y, An Q, Mei Z, Xu Q, Ding Y, Zhao G, Guo H (2023) Regulating the lithium ions' local coordination environment through designing a COF with single atomic Co site to achieve dendrite-free lithium-metal batteries. Adv Mater 35: 2304511. https://doi.org/10.1002/adma.202304511

[25] Cheng R, Xian X, Manasa P, Liu J, Xia Y, Guan Y, Wei S, Li Z, Li B, Xu F, Sun L (2022) Carbon coated metal-based composite electrode materials for Lithium sulfur batteries: A Review. Chem Rec 22(10): e202200168. https://doi.org/10.1002/tcr.202200168

[26] Wu B, Shan C, Zhang X, Zhao H, Ma S, Shi Y, Yang J, Bai H, Liu Q (2021) CeO_2/Co_3O_4 porous nanosheet prepared using rose petal as biotemplate for photo-catalytic degradation of organic contaminants. Appl Surf Sci 543: 148677. https://doi.org/10.1016/j.apsusc.2020.148677

[27] Wang X, Huang F, Rong F, He P, Que R, Jiang S (2019) Unique MOF-derived hierarchical MnO_2 nanotubes@NiCo-LDH/CoS_2 nanocage materials as high performance supercapacitors. J Mater Chem A 7: 12018-12028. https://doi.org/10.1039/C9TA01951K

[28] Liu X, He Q, Wang Y, Wang J, Xiang Y, Blackwood D, Wu R, Chen J (2020) MOF-reinforced Co_9S_8 self-supported nanowire arrays for highly durable and flexible supercapacitor. Electrochim Acta 346: 136201. https://doi.org/10.1016/j.electacta.2020.136201

[29] Mu G, Zeng Y, Zheng Y, Cao Y, Liu F, Liang S, Zhan Y, Jiang L (2023) Oxygen vacancy defects engineering on Cu-doped Co_3O_4 for promoting effective COS hydrolysis. Green Energy Environ 8: 831-841. https://doi.org/10.1016/j.gee.2021.11.001

[30] Yan Z, Sun Z, Qiu Y, Guo Z, Liu H, Wang P, Tian S, Ding H, Du B, Qian L (2022) In situ F doping-induced multilayer FeS_2@CoS@C hierarchical heterostructures for ultrafast lithium

storage. Mater Today Energy 29: 101108. https://doi.org/10.1016/j.mtener.2022.101108

[31] Zhang Y, Wang N, Sun C, Lu Z, Xue P, Tang B, Bai Z, Dou S (2018) 3D spongy CoS_2 nanoparticles/carbon composite as high-performance anode material for lithium/sodium ion batteries. Chem Eng J 332: 370-376. https://doi.org/10.1016/j.cej.2017.09.092

[32] Chen X, Wang P, Zhang Z, Yin L (2020) Bi_2S_3-CoS@C core-shell structure derived from ZIF-67 as anodes for high performance lithium-ion batteries. J Alloy Compd 844: 156008. https://doi.org/10.1016/j.jallcom.2020.156008

[33] Liu Z, Peng H, Xie X, Wang X, Pu Y, Ma G, Lei Z (2022) One-step self-embedding of CoP nanoparticles in N, P-codoped hard carbon for high-performance lithium-ion capacitors. J Power Sources 543: 231831. https://doi.org/10.1016/j.jpowsour.2022.231831

[34] Zhao C, Zhang L, Jing S, Kong S, Zhang X, Lan X, Feng Y, Liu C, Tian K, Gong W, Li Q (2023) In situ construction of heterostructured Co_3O_4/CoP nanoflake arrays on carbon cloth as binder-free anode for high-performance lithium-ion batteries. ACS Appl Mater Interfaces 15: 23217-23225. https://doi.org/10.1021/acsami.3c02455

[35] Guo J, Jiang H, Yu M, Li X, Dai Y, Zheng W, Jiang X, He G (2022) Sandwich-Structured flexible interlayer with Co_3O_4 nanoboxes strung along carbon nanofibers on both sides for fast Li+ transport and high redox activity in High-Rate Li-S batteries. Chem Eng J 449: 137777. https://doi.org10.1016/j.cej.2022.137777

[36] Zhao M, Peng H J, Li B, Chen X, Xie J, Liu X, Zhang Q, Huang J (2020) Electrochemical phase evolution of metal-based pre-catalysts for high-rate polysulfide conversion. Angew Chem 132: 9193. https://doi.org/10.1002/anie.202005704

[37] Zhang B, Zhao S, Tang Z, Xie P, Natarajan A, Zhou Y, Tian X (2022) High-performance three-dimensional flower-like CoS/MWCNT composite host for Li-S batteries. J Solid State Electr 26: 389-400. https://doi.org/10.1007/s10008-021-05066-x

[38] Yuan H, Wang F, Li S, Lin Z, Huang J (2020) A cellulose substance derived nanofibrous CoS-nanoparticle/carbon composite as a high-performance anodic material for lithium-ion batteries. New J Chem 44: 1846-1857. https://doi.org/10.1039/C9NJ05587H

[39] Jin G, Liu D, Hu K, Hu K, Sun S, Wu H, Fu N, Chen J (2024) Lithium-Rich layered oxide cathode materials modified for Lithium-ion batteries by CoS of a 3D rock salt structure assisted by PVP. ACS Appl Mater Interfaces 16: 70520-70530. https://doi.org/10.1021/acsami.4c15367

Supplementary Files

This is a list of supplementary files associated with this preprint. Click to download.

- SupportingInformation1.doc